photonics

Communication

Tight Focusing Properties of Ring Pearcey Beams with a Cross Phase

Chaoqun Yu [1,†], Zhimin He [1,†], Cheng Huang [1], Fuchang Chen [1], Jun Zeng [1], Yan Li [1], Yongtao Zhang [1], Jixiong Pu [1,2] and Huichuan Lin [1,*]

1 College of Physics and Information Engineering, Minnan Normal University, Zhangzhou 363000, China
2 Fujian Provincial Key Laboratory of Light Propagation and Transformation, College of Information Science & Engineering, Huaqiao University, Xiamen 361021, China
* Correspondence: lhc1810@mnnu.edu.cn; Tel.: +86-18-8763-30655
† These authors contributed equally to this work.

Abstract: We theoretically investigated the properties of tightly focused ring Pearcey beams with a cross phase (CPRPB). The expressions of the distributions of both electric field and magnetic field in the focal region of an objective were first derived from the vectorial Debye theory, and then numerical calculations were carried out to obtain the focused intensity distribution and the Poynting vector of CPRPB near the focus. Numerical calculations indicate that as CPRPB is focused on an objective of high numerical aperture (NA), two nonuniform self-focusing spots occur at both sides of the geometrical focus of the objective symmetrically, and the angle between their directions is 90 degrees. The stronger is the strength of cross-phase modulation, the flatter are the ellipses of the self-focusing spots, and the smaller is the intensity at the geometrical focus of the objective. Numerical calculations also demonstrate that the optical gradient force produced by tightly focused CPRPB in the focal region can be manipulated in magnitude and in direction by tuning the strength of cross-phase modulation. Due to these properties of tightly focused CPRPB, they might find applications in the manipulation of micro- and nanoparticles and so on.

Keywords: cross phase; Pearcey beams; tight focusing; self-focusing

Citation: Yu, C.; He, Z.; Huang, C.; Chen, F.; Zeng, J.; Li, Y.; Zhang, Y.; Pu, J.; Lin, H. Tight Focusing Properties of Ring Pearcey Beams with a Cross Phase. *Photonics* **2022**, *9*, 964. https://doi.org/10.3390/photonics9120964

Received: 27 October 2022
Accepted: 7 December 2022
Published: 10 December 2022

1. Introduction

Taking advantage of focusing energy at a point along the propagation of light beams, self-focusing beams have found applications in many scenarios. In laser medicine, for instance, self-focusing beams maintain low power during propagation, avoiding the damage of tissues outside the region of interest [1]. Considerable optical gradient force can be produced by the self-focusing beams to trap or manipulate the micro- and nanoscale particles accurately [2,3]. Therefore, self-focusing beams always attract the keen interests of researchers [4–9]. Ring Pearcey beams were first reported by Chen et al., in 2018, and it was indicated that ring Pearcey beams belonged to a family of self-focusing beams. Compared with other self-focusing beams, ring Pearcey beams are characterized by their higher peak intensity contrast, shorter focal length, and no oscillatory energy loss beyond focus [10]. Cross phase is a unique phase structure. By cross-phase modulation, interconversion between the Hermite–Gaussian (HG) modes and rotation of the partially coherent Gaussian-Schell model beams can be realized [11–13]. Cross-phase modulation can also be employed to generate, to measure, and to manipulate high-order optical vortices [14,15]. To investigate the propagation of modulated laser beams, cross-phase modulation was utilized by Liu et al. in 2021 to modulate the ring Pearcey beams, and the ring Pearcey beams with a cross phase (CPRPB) was developed. It was found that CPRPB's focal length, direction, rotation angle, and symmetry of their self-focusing spots can be flexibly changed by cross-phase modulation [6].

Subwavelength focal spots can be achieved by focusing the laser beams with an objective of high numerical aperture (NA). Laser beams can also be shaped by modulating the polarization property, phase distribution, and coherent characteristics of the incident beams. These beam-shaping schemes are desirable for many applications, such as optical data storage, microscope, particle capture, and material processing. Thus, many research efforts have been made to study the tight-focusing properties of the laser beams of different types in these years [16–24]. Considering the self-focusing property and unique phase structure of CPRPB, it will be a significant work to explore its tight-focusing properties. Based on the Richards-Wolf vector diffraction theory, in this paper, the electric field and intensity distributions of CPRPB tightly focused on an objective of high NA in the focal region were derived. The gradient forces imposed on micro- and nanoparticles by the focused beams were computed, and the influence of cross-phase on the self-focusing spots and optical gradient forces was discussed.

2. Theoretical Analysis

The electric field in the source plane of CPRPB can be expressed as

$$\begin{aligned} E(x,y,z=0) =& \, \mathrm{Pe}(\gamma,-r/p) \\ &\times \exp\left\{-\alpha r^2 + i\mu[x\cos\delta - y\sin\delta]\times[x\sin\delta + y\cos\delta]\right\} \end{aligned} \tag{1}$$

where $r = \sqrt{x^2+y^2}$ is the modulus in the polar coordinate system of the source plane, $\mathrm{Pe}(\gamma, -r/p)$ is the Pearcey function, γ and p are the factors that affect the spatial distribution of the light intensity, α is the attenuation factor that guarantees finite beam energy, μ is a real coefficient that determines the intensity of cross-phase modulation, and δ is the azimuth parameter that determines the autofocus orientation [12].

As illustrated in Figure 1, CPRPB is tightly focused on an objective lens of high NA. According to the vectorial Debye theory [25], the field distribution in the region of the objective's geometrical focus can be expressed as

$$\begin{aligned} E(\rho,\psi,z) =& \frac{iE_0}{\lambda}\int_0^{\beta}\int_0^{2\pi} \exp[-ikz\cos\theta - ik\rho\sin\theta\cos(\psi-\varphi)] \\ &\times P(\varphi,\theta)K(\varphi,\theta)\sin\theta\sqrt{\cos\theta}d\varphi d\theta \end{aligned} \tag{2}$$

where θ is the angle of refraction, λ is the wavelength of the beam, k is the wavenumber, $\beta = \sin^{-1}$ (NA) is the maximum angle of refraction that is decided by the numerical aperture of the objective, E_0 is a constant here representing the amplitude of the incident beam and the variables, and ρ, ψ, and z are the cylindrical coordinates in the focal region. Assume that the incident CPRPB are the linearly polarized beams, $k(\varphi, \theta)$, in Equation (2):

$$K(\varphi,\theta) = \begin{bmatrix} (\cos\theta + \sin^2\varphi(1-\cos\theta))\boldsymbol{e_x} \\ \cos\varphi\sin\varphi(\cos\theta-1)\boldsymbol{e_y} \\ \cos\varphi\sin\theta\boldsymbol{e_z} \end{bmatrix} \tag{3}$$

where $\boldsymbol{e_x}$, $\boldsymbol{e_y}$, and $\boldsymbol{e_z}$ are the unit vectors along the x, y, and z axes in the Cartesian coordinate system of the focal region. By projecting the incident CPRPB to the aperture of the objective, the apodization function of CPRPB at the objective can be obtained from Equation (1) as

$$\begin{aligned} P(\varphi,\theta) =& \, \mathrm{Pe}(\gamma,-f\sin\theta/p)\exp\left(-\alpha(f\sin\theta)^2\right) \\ &\times \exp\{i\mu f\sin\theta[\cos\varphi\cos\delta - \sin\varphi\sin\delta] \\ &\times f\sin\theta[\cos\varphi\sin\delta + \sin\varphi\cos\delta]\} \end{aligned} \tag{4}$$

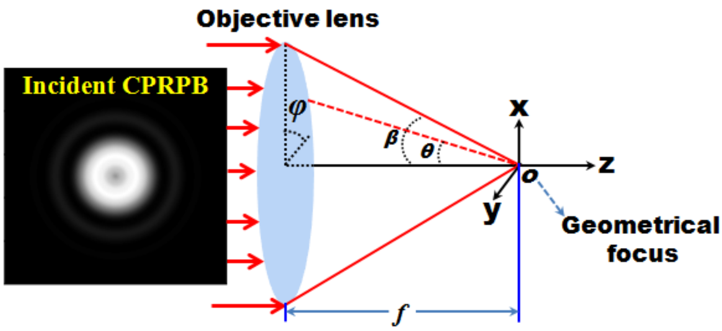

Figure 1. Intensity distribution of incident linearly polarized CPRPB (left) and schematic of a tight-focusing setup (right).

Put $k(\varphi, \theta)$ in Equation (3) and $P(\varphi, \theta)$ in Equation (4) into Equation (2) and set $\delta = 0$. Three polarized components of the electric field distribution of tightly focused CPRPB in the focal region of the objective of high NA are achieved in Cartesian coordinates as

$$\begin{aligned} E_x(\rho,\psi,z) = & \frac{\pi E_0}{2\lambda}\int_0^\beta \mathrm{Pe}(\gamma,-f\sin\theta/p)\exp\left[-\alpha f^2\sin^2\theta - ikz\cos\theta\right] \\ & \times \sin\theta \sum_{l=-\infty}^{\infty} i^{-l} J_l\left(\frac{1}{2}\mu f^2\sin^2\theta\right)\exp\left(-il\frac{\pi}{2}\right)\exp(2il\psi) \\ & +\{2J_{2l}(k\rho\sin\theta)(\cos\theta+1)\,J_{2l+2}(k\rho\sin\theta)\exp(2i\psi)(1-\cos\theta) \\ & +J_{2l-2}(k\rho\sin\theta)\exp(-2i\psi)(1-\cos\theta)\}d\theta \end{aligned} \tag{5}$$

$$\begin{aligned} E_y(\rho,\psi,z) = & \frac{\pi E_0(1-\cos\theta)}{2\lambda}\int_0^\beta \mathrm{Pe}(\gamma,-f\sin\theta/p)\exp\left[-\alpha f^2\sin^2\theta - ikz\cos\theta\right] \\ & \times \sin\theta \sum_{l=-\infty}^{\infty} i^{-(l+1)} J_l\left(\frac{1}{2}\mu f^2\sin^2\theta\right)\exp\left(-il\frac{\pi}{2}\right)\exp(2il\psi) \\ & \times\{J_{2l+2}(k\rho\sin\theta)\exp(2i\psi) - J_{2l-2}(k\rho\sin\theta)\exp(-2i\psi)\}d\theta \end{aligned} \tag{6}$$

$$\begin{aligned} E_z(\rho,\psi,z) = & \frac{-\pi E_0}{\lambda}\int_0^\beta \mathrm{Pe}(\gamma,-f\sin\theta/p)\exp\left[-\alpha f^2\sin^2\theta - ikz\cos\theta\right] \\ & \times \sin^2\theta \sum_{l=-\infty}^{\infty} i^{-(l+1)} J_l\left(\frac{1}{2}\mu f^2\sin^2\theta\right)\exp\left(-il\frac{\pi}{2}\right)\exp(2il\psi) \\ & \times\{J_{2l+1}(k\rho\sin\theta)\exp(i\psi) + J_{2l-1}(k\rho\sin\theta)\exp(-i\psi)\}d\theta \end{aligned} \tag{7}$$

With Equations (5)–(7), it is feasible to study the properties of CPRPB focused on an objective of high NA. In order to illustrate the effect of cross-phase modulation on the properties of tightly focused CPRPB more explicitly, numerical calculations were carried out utilizing the derived equations above, concentrating on the influence of the intensity factor of cross-phase modulation, μ, on the focused beams.

3. Results and Discussions

Based on the field distribution equations derived previously, the intensity distributions in the focal plane of the objective were first computed and are illustrated in Figure 2. Figure 2a indicates the x-polarization component, Figure 2b indicates the z-polarization component (longitudinal field), and Figure 2c indicates the y-polarization component. It could be found out from these figures that CPRPB was depolarized as focused on an objective of high NA. The intensity of the y-polarization component is about one thousandth of the intensity of the x-polarization component, while the intensity of the z-polarization component is about one millionth of that of the x-polarization component. As shown in Figure 2c, the y-polarization component appears as a doughnut-shaped ring. There exists a phase singularity at the center of the ring, illustrated by the color inset in the upper-left corner of Figure 2c, which was obtained by computing the phase distribution of this component. Figure 2d is the total intensity distribution of three components. Since the intensity of the x-polarization component far outweighs that of the y- and z-polarization components, the total intensity distribution seems similar to the intensity distribution of the x-polarization component.

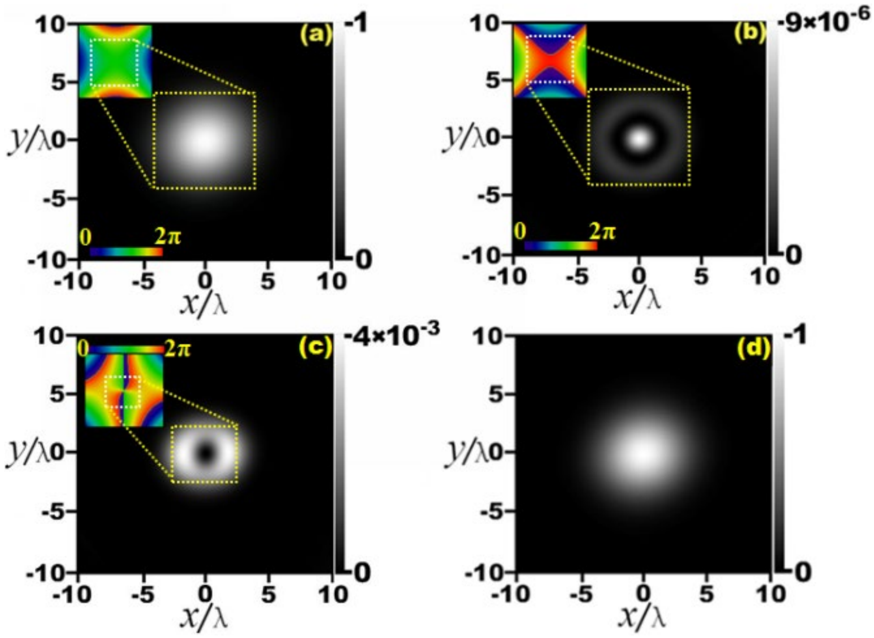

Figure 2. Intensity distributions in focal plane, (**a**) x-polarization component, (**b**) z-polarization component, (**c**) y-polarization component, (**d**) total intensity. Parameters for calculation are chosen as λ = 633 nm, α = 3, NA = 0.9, f = 3.4 cm, μ = 10 mm^{-2}, and E_0 = 1.

Figure 3 indicates the intensity distributions of tightly focused CPRPB in the ρ-z planes around the focus of the objective, in which (a), (b), (c), and (d) are the intensity distributions in the planes of ψ = 0, ψ = $\pi/4$, ψ = $\pi/2$, and ψ = $3\pi/4$, respectively. It can be concluded from the figures that the focused beam is axially asymmetrical in the region around the focus, and the maxima are not located at the geometrical focus of the objective, as CPRPB is tightly focused.

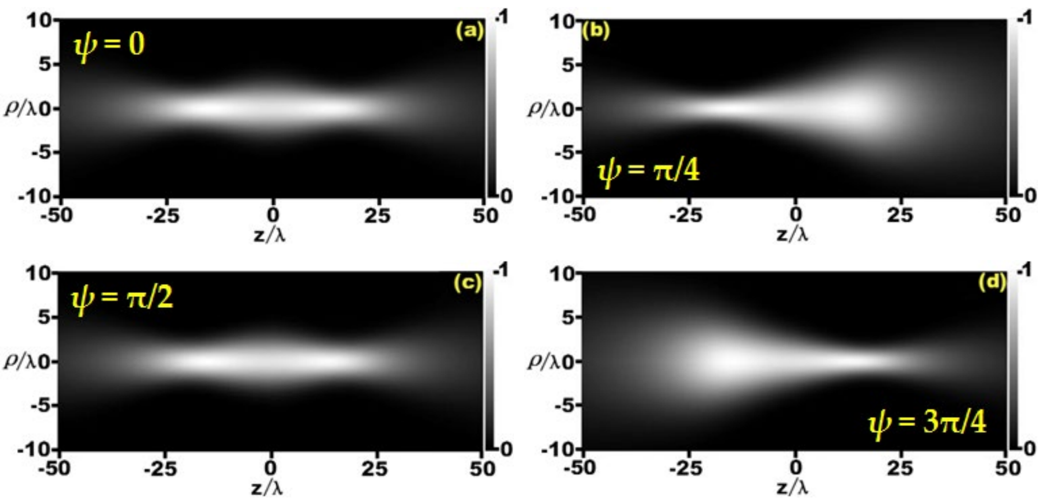

Figure 3. Intensity distributions in ρ-z planes around the focus. (**a**) ψ = 0, (**b**) ψ = $\pi/4$, (**c**) ψ = $\pi/2$, and (**d**) ψ = $3\pi/4$. Parameters for calculation are chosen as λ = 633 nm, α = 3, NA = 0.9, f = 3.4 cm, μ = 10 mm^{-2}, and E_0 = 1.

In order to find out the reason for the asymmetry of the focused beam and deviation of the maxima from the focus, intensity distributions of tightly focused CPRPB in the cross sections around the focal plane were computed and are listed in Figure 4 according to the sequence of beam propagation. The subdiagrams, (a)–(g), are the intensity distributions in the planes of (a) $z = -34\lambda$, $z = -17\lambda$, $z = -7\lambda$, $z = 0$, $z = 7\lambda$, $z = 17\lambda$, and $z = 34\lambda$, respectively. The plane of $z = 0$ is the focal plane as well. Numerical results show that the self-focusing phenomenon occurs twice as CPRPB tightly focused on the objective. One self-focusing is prior to the focus, and the other is behind the focus. The angle between their directions is 90 degrees. Therefore, it can be concluded that the beam rotates as it travels through the focal region. Two self-focusings separated at both sides of the geometrical focus of the objective and rotation of the beam lead to the asymmetry of intensity distribution. In addition, Figure 4b shows that the major radius of the elliptical beam profile has an inclination angle of 135° from the x-axis, which is in agreement with the experimental result shown in Reference [6]. Figure 4h plots the ratio of the major radius to the minor radius of the elliptical beam profile versus its position in the optical axis. It can be seen clearly from the curve that the beam's cross section deforms from an elliptical shape to a circular shape, and then back to an ellipse during propagation. Elliptical Gaussian beam takes a similar characteristic of asymmetric self-focusing during propagation; therefore, it might have the same manner of beam deformation as it is tightly focused. Asymmetrical intensity distribution and rotation of the beam in the focal region results in rotational intensity gradient distribution, and thus an optical torque, which might play an important role in optical manipulation.

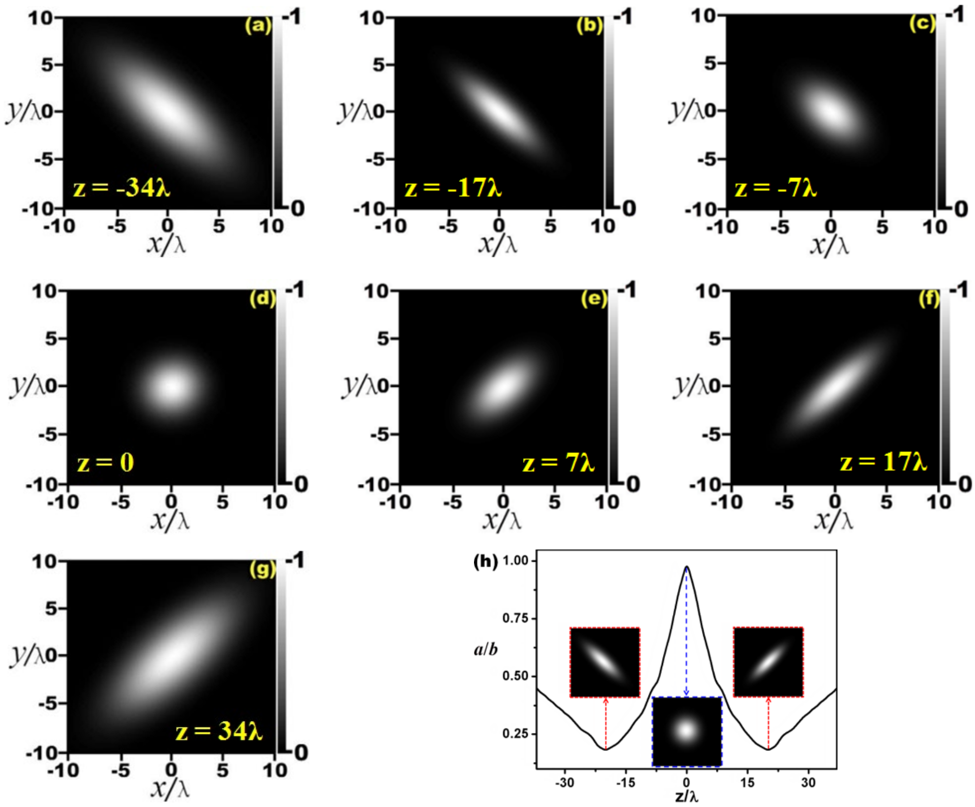

Figure 4. Intensity distributions in different cross sections around the focus, (**a**) $z = -34\lambda$, (**b**) $z = -17\lambda$, (**c**) $z = -7\lambda$, (**d**) $z = 0$, (**e**) $z = 7\lambda$, (**f**) $z = 17\lambda$, and (**g**) $z = 34\lambda$; (**h**) the ratio of the major radius to the minor radius of the elliptical beam profile versus its position in the optical axis. Parameters for calculation are chosen as $\lambda = 633$ nm, $\alpha = 3$, NA = 0.9, $f = 3.4$ cm, $\mu = 10$ mm^{-2}, and $E_0 = 1$.

It was reported that cross-phase modulation altered the symmetry of the intensity distributions of ring Pearcey beams, which could have affected their optical trapping capability. Therefore, it is essential to figure out the effect of the cross-phase modulation on the properties of tightly focused CPRPB. Figure 5 illustrates the intensity distributions of the self-focusing spots of tightly focused CPRPB modulated with different cross-phase modulation intensities. According to the ratio of the major radius to the minor radius of the beam profiles (a/b) in the subdiagrams in Figure 5, it can be seen that the stronger is the cross-phase modulation, the flatter is the ellipse of the beam profile. This conclusion is in good agreement with the practical results illustrated in Reference [6], which proves that the theoretical derivation is correct. With the intensity modulation factor, μ, reduced to 5 mm^{-2}, the beam profile is pretty close to a circle. Provided that the self-focusing spot of a ring Pearcey beam is exactly a circle, the beam does not rotate in the focal region as it is tightly focused. In this case, there exists no optical torque when it is employed as optical tweezers. In brief, in the manipulation of micro- and nanoparticles by tightly focused CPRPB, the optical torque in the focal region can be tuned by altering the intensity of the cross-phase modulation.

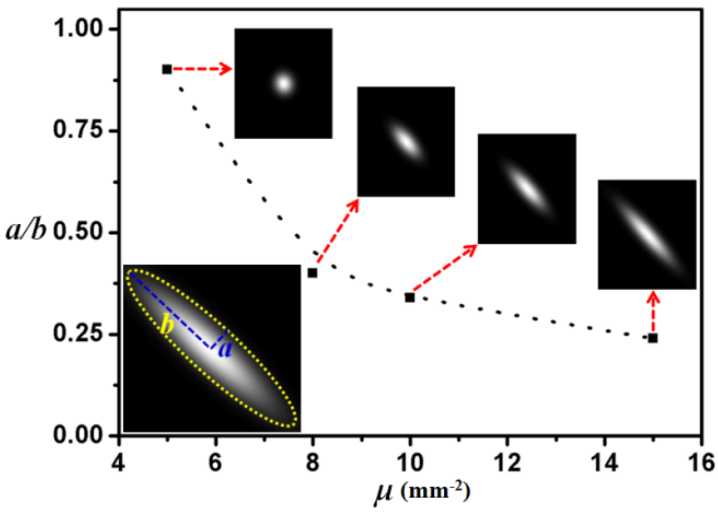

Figure 5. Influence of the cross-phase modulation on the intensity distribution of self-focusing spots. Parameters for calculation are chosen as λ = 633 nm, α = 3, NA = 0.9, f = 3.4 cm, and E_0 = 1.

As discussed previously, the maximum intensity of tightly focused CPRPB in the focal region is not located at the geometrical focus of the objective due to their self-focusing property, and cross-phase modulation also affects the intensity distributions of their self-focusing spots. In the optical trapping of micro- and nanoparticles, particles are usually trapped at the point of intensity maximum by the optical gradient force, where the optical gradient force is equal to zero [26]. According to different intensities of cross-phase modulation, the intensity distributions along the optical axis were calculated and are plotted in Figure 6. With relatively mild modulation intensity (μ = 5 mm^{-2}), the intensity of the beam focused on an objective of high NA peaks at the geometrical focus of the objective. As modulation intensity increases, the intensity distribution profile takes a saddle shape in which the intensity maxima shift towards both sides of the geometrical focus, while the saddle point located at the focus moves down. When the intensity factor of cross-phase modulation, μ, equals 18 mm^{-2}, the intensity of the tightly focused beam at the geometrical focus of the objective falls to zero.

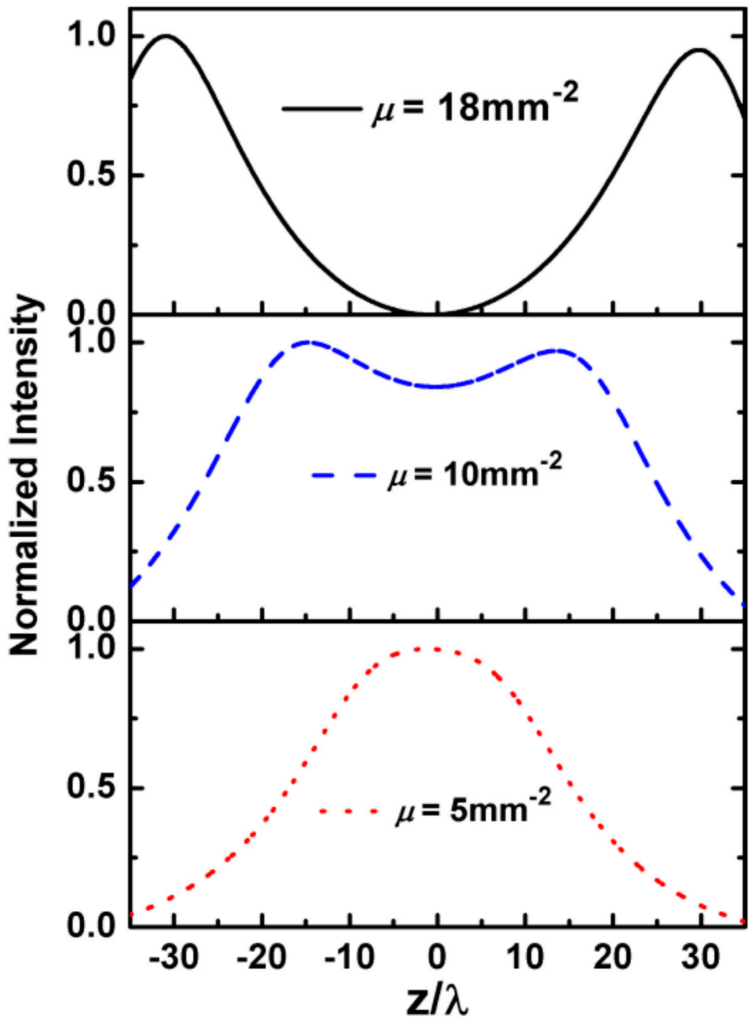

Figure 6. Influence of cross-phase modulation on the intensity distribution along the optical axis. Parameters for calculation are chosen as λ = 633 nm, α = 3, NA = 0.9, f = 3.4 cm, and E_0 = 1.

It can be concluded from the calculations above that the cross-phase modulation plays a key role in the intensity distribution of the ring Pearcey beams in the focal region. In the study of how the change of intensity distribution affects the optical trapping of micro- and nanoparticles, the gradient forces produced by tightly focused CPRPB on the particles were calculated through Equation (8). For simplicity, it was assumed that the radii of the particles trapped were far smaller than the wavelength of the focused beam.

$$\boldsymbol{F}_g(\rho,\psi,z) = 2\pi a^3 \frac{n_2}{c}\frac{m^2-1}{m^2+2}\nabla I(\rho,\psi,z) \tag{8}$$

In Equation (8), $I(\rho, \psi, z)$ is the intensity distribution of CPRPB in the focal region, a is the radius of the trapped particle, n_2 is the refractive index of the particle, n_1 is the refractive index of the background medium, $m = n_2/n_1$, and c is the speed of light in vacuum. The formula of optical gradient force of Equation (8) implies that the intensity gradients are zero at the intensity maxima, and thus the gradient forces produced by the beam at those points are nil as well. As the refractive index of a particle is greater than the refractive index of the background medium, that is, $n_2 > n_1$, the particle would have been trapped at the positions of intensity maxima, which are usually located at the optical axis of the beam. The gradient forces along the optical axis of the tightly focused CPRPB with reference to different intensities of cross-phase modulation were calculated and are plotted in Figure 7. Numerical results explicitly show that there exists a balance point of zero gradient force formed at the geometrical focus of the objective regardless of the modulation intensity. However, the gradient force along the axis varies acutely with the increase in cross-phase modulation intensity. With μ equaling 5 mm^{-2}, the gradient force is positive on the left side of the focus while negative on the right side. When μ rises to 10 mm^{-2}, the profile of gradient force is flipped vertically. Meanwhile, another two balance points of zero gradient force appear at distances of $\pm 15\lambda$ from the geometrical focus in the optical axis. As the modulation intensity increases further, two new balance points move farther away from the focus, and the profile of gradient force is flipped vertically again. Besides intensity distribution and gradient force, the Poynting vector that describes the energy flows of a beam would be affected by the cross-phase modulation as well. Based on the studies in [27–29], it is meaningful to study the Poynting vector of tightly focused CPRPB.

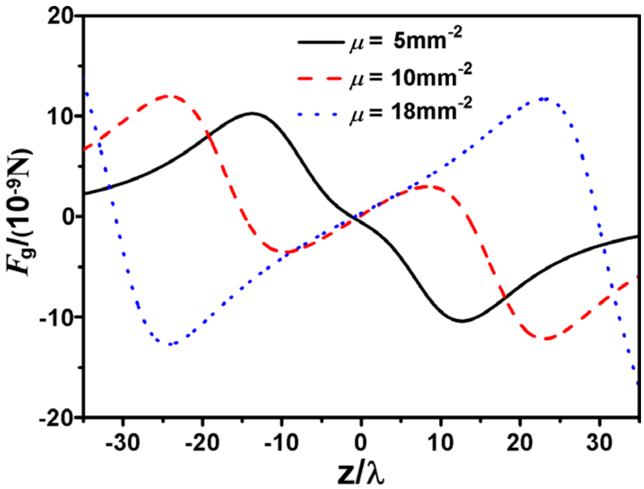

Figure 7. Influence of cross-phase modulation on the gradient force along the optical axis. Parameters for calculation are chosen as λ = 633 nm, α = 3, NA = 0.9, f = 3.4 cm, n_2 = 1.5, n_1 = 1.3, and a = 20 nm, $E_0 = \sqrt{100(\text{mW}/\text{um}^2)}$.

The Poynting vector is another important characteristic of a beam indicating the beam's energy flows. The Poynting vector can be expressed as $S = E \times H$, in which E and H are the electric and magnetic field vectors, respectively. In order to study the Poynting vector, both E and H have to be solved. The magnetic field distribution of the linearly polarized CPRPB in the focal region is expressed as

$$B(\rho,\psi,z) = \frac{iB_0}{\lambda}\int_0^{\beta}\int_0^{2\pi}\exp[-ikz\cos\theta - ik\rho\sin\theta\cos(\psi-\varphi)] \times P(\varphi,\theta)\begin{Bmatrix}\sin\varphi\cos\varphi(\cos\theta-1)\boldsymbol{e_x}\\ [\cos\theta+\cos^2\varphi(1-\cos\theta)]\boldsymbol{e_y}\\ \sin\varphi\sin\theta\boldsymbol{e_z}\end{Bmatrix}\sin\theta\sqrt{\cos\theta}d\varphi d\theta \tag{9}$$

By solving Equation (9), three polarized components of the magnetic field distribution of the tightly focused linearly polarized CPRPB in the focal region are achieved in Cartesian coordinates as

$$\begin{aligned} B_x(\rho,\psi,z) = {} & \frac{\pi B_0(1-\cos\theta)}{2\lambda}\int_0^{\beta}\text{Pe}(\gamma,-f\sin\theta/p)\exp\left[-\alpha f^2\sin^2\theta - ikz\cos\theta\right] \\ & \times\sin\theta\sum_{l=-\infty}^{\infty} i^{-(l+1)}J_l\left(\frac{1}{2}\mu f^2\sin^2\theta\right)\exp\left(-il\frac{\pi}{2}\right)\exp(2il\psi) \\ & \times\{J_{2l+2}(k\rho\sin\theta)\exp(2i\psi) - J_{2l-2}(k\rho\sin\theta)\exp(-2i\psi)\}d\theta \end{aligned} \tag{10}$$

$$
\begin{aligned}
B_y(\rho,\psi,z) = {} & \frac{\pi B_0}{2\lambda}\int_0^\beta \mathrm{Pe}(\gamma,-f\sin\theta/p)\exp\left[-\alpha f^2\sin^2\theta - ikz\cos\theta\right] \\
& \times \sin\theta \sum_{l=-\infty}^{\infty} i^{-l} J_l\left(\frac{1}{2}\mu f^2\sin^2\theta\right)\exp\left(-il\frac{\pi}{2}\right)\exp(2il\psi) \\
& + \{2J_{2l}(k\rho\sin\theta)(\cos\theta+1)\, J_{2l+2}(k\rho\sin\theta)\exp(2i\psi)(\cos\theta-1) \\
& + J_{2l-2}(k\rho\sin\theta)\exp(-2i\psi)(\cos\theta-1)\}d\theta
\end{aligned}
\tag{11}
$$

$$
\begin{aligned}
B_z(\rho,\psi,z) = {} & \frac{-\pi B_0}{\lambda}\int_0^\beta \mathrm{Pe}(\gamma,-f\sin\theta/p)\exp\left[-\alpha f^2\sin^2\theta - ikz\cos\theta\right] \\
& \times \sin^2\theta \sum_{l=-\infty}^{\infty} i^{-l} J_l\left(\frac{1}{2}\mu f^2\sin^2\theta\right)\exp\left(-il\frac{\pi}{2}\right)\exp(2il\psi) \\
& \times \{J_{2l+1}(k\rho\sin\theta)\exp(i\psi) - J_{2l-1}(k\rho\sin\theta)\exp(-i\psi)\}d\theta
\end{aligned}
\tag{12}
$$

Three polarized components of the electric filed distribution are shown in Equations (5)–(7). Numerical calculations were then applied to these equations, and the distributions of the Poynting vector of the tightly focused CPRPB were achieved, as shown in Figure 8.

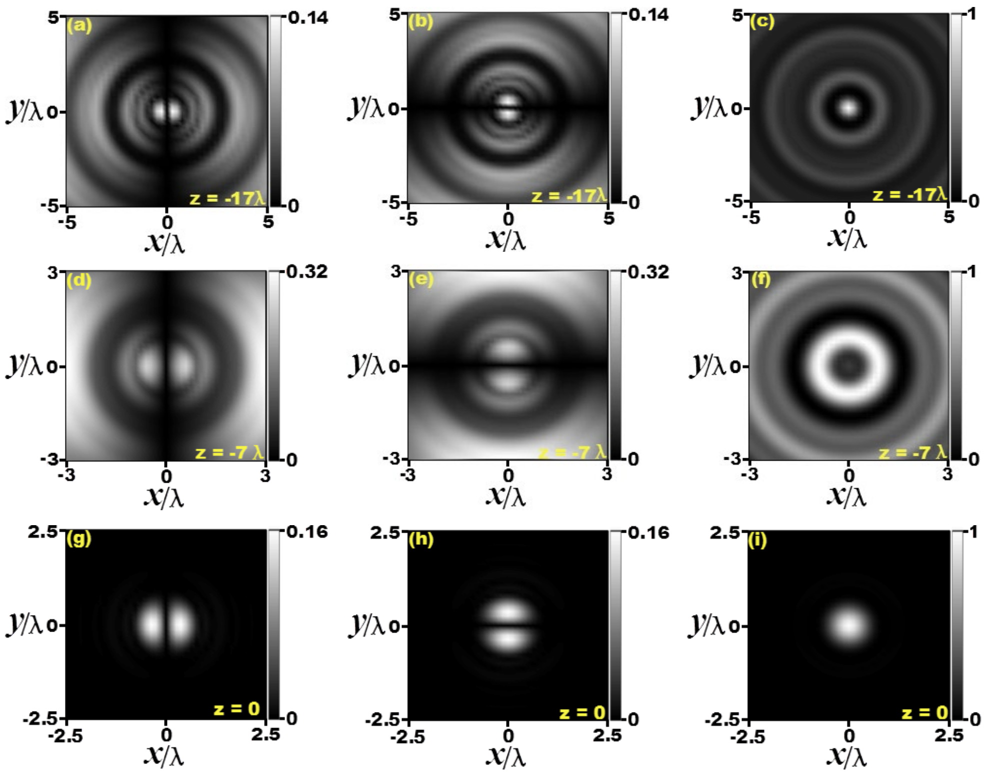

Figure 8. Poynting vector distributions in different cross sections around the focus. (**a**,**d**,**g**) are S_x; (**b**,**e**,**h**) are S_y; and (**c**,**f**,**i**) are S_z. Parameters for calculation are chosen as λ = 633 nm, α = 3, NA = 0.9, f = 3.4 cm, μ = 10 mm^{-2}, and $E_0 = B_0 = 1$.

It can been found from Figure 8 that there exist lateral energy flows (S_x and S_y) in the focal region, besides the energy flow along the optical axis (S_z). However, the ratios of S_x and S_y to S_z vary with the position. At the self-focusing position, that is, z = −17λ, the ratios of S_x and S_y to S_z are 0.14, while at the positions of z = −7λ and z = 0, the ratios are 0.32 and 0.16, respectively.

4. Concluding Remarks

The properties of tightly focused CPRPB were presented in this paper, focusing on the influences of the cross-phase modulation intensity on the intensity distribution of the focused beam and on the optical gradient force produced along the optical axis of the beam. Numerical results show that nonuniform self-focusing phenomena occur at both sides of the geometrical focus of the objective, and the angle between the directions of two self-focusing spots is 90 degrees, as CPRPB is tightly focused on an objective of high NA. The intensity of cross-phase modulation plays a key role in the properties of tightly focused beams. The stronger is the modulation strength, the flatter are the ellipses of the self-focusing spots beside the focal plane and the smaller is the intensity at the focus of the objective. The study of gradient forces along the optical axis in different intensities of cross-phase modulation demonstrates that the optical gradient force produced by tightly focused CPRPB in the focal region can be manipulated in magnitude and in direction by tuning the modulation intensity. Due to these properties of tightly focused CPRPB, they might find use in the manipulation of micro- and nanoparticles.

Funding: This research was funded by National Natural Science Foundation of China (NSFC), grant numbers 61975072 and 12174173; This research was funded by Natural Science Foundation of Fujian province, grant numbers 2022H0023, 2022J02047 and 2022G02006; This research was funded by the Young Core Instructor from the Education Department of Fujian Province, grant numbers JT180295 and JAT190393.

Institutional Review Board Statement: Not applicable.

Informed Consent Statement: Not applicable.

Conflicts of Interest: No conflict of interest exits in this manuscript, and manuscript is approved by all authors.

References

1. Ioannis, C.; Efremidis, N.; Christodoulides, D. Pre-engineered abruptly autofocusing beams. *Opt. Lett.* **2011**, *36*, 1890–1892.
2. Jiang, Y.; Huang, K.; Lu, X. Radiation force of abruptly autofocusing Airy beams on a Rayleigh particle. *Opt. Express* **2013**, *21*, 24413–24421. [CrossRef] [PubMed]
3. Lu, W.; Sun, X.; Chen, H.; Liu, S.; Lin, Z. Abruptly autofocusing property and optical manipulation of circular Airy beams. *Phys. Rev. A* **2019**, *99*, 013817. [CrossRef]
4. Efremidis, N.K.; Christodoulides, D.N. Abruptly autofocusing waves. *Opt. Lett.* **2010**, *35*, 4045–4047. [CrossRef]
5. Manousidaki, M.; Papazoglou, D.; Farsari, M.; Tzortzakis, S. Abruptly autofocusing beams enable advanced multiscale photo-polymerization. *Optica* **2016**, *3*, 525–530. [CrossRef]
6. Xin, L.; Li, Z.; Monfared, Y.E.; Liang, C.; Wang, F.; Hoenders, B.J.; Cai, Y.; Ma, P. Flexible autofocusing properties of ring Pearcey beams by means of a cross phase. *Opt. Lett.* **2021**, *46*, 70–73. [CrossRef]
7. Ding, C.; Korotkova, O.; Horoshko, D.; Zhao, Z.; Pan, L. Evolution of Spatiotemporal Intensity of Partially Coherent Pulsed Beams with Spatial Cosine-Gaussian and Temporal Laguerre–Gaussian Correlations in Still, Pure Water. *Photonics* **2021**, *8*, 102. [CrossRef]
8. Chen, K.H.; Qiu, H.X.; Wu, Y.; Lin, Z.; Huang, H.; Shui, L.; Deng, D.; Liu, H.; Chen, Z. Generation and control of dynamically tunable circular Pearcey beams with annular spiral-zone phase. *Sci. China Phys. Mech. Astron.* **2021**, *64*, 104211. [CrossRef]
9. Xu, D.; Mo, Z.; Jiang, J.; Huang, H.; Wei, Q.; Wu, Y.; Wang, X.; Liang, Z.; Yang, H.; Chen, H.; et al. Guiding particles along arbitrary trajectories by circular Pearcey-like vortex beams. *Phys. Rev. A* **2022**, *106*, 013509. [CrossRef]
10. Chen, X.; Deng, D.; Zhuang, J.; Peng, X.; Li, D.; Zhang, L.; Zhao, F.; Yang, X.; Liu, H.; Wang, G. Focusing properties of circle Pearcey beams. *Opt. Lett.* **2018**, *43*, 3626–3629. [CrossRef]
11. Liang, G.; Wang, Q. Controllable conversion between Hermite Gaussian and Laguerre Gaussian modes due to cross phase. *Opt. Express* **2019**, *27*, 10684–10691. [CrossRef]
12. Wan, L.; Zhao, D. Controllable rotating Gaussian Schell-model beams. *Opt. Lett.* **2019**, *44*, 735–738. [CrossRef]
13. Liu, Z.; Zhao, D. Experimental generation of a kind of reversal rotating beams. *Opt. Express* **2020**, *28*, 2884–2894. [CrossRef] [PubMed]
14. Shen, D.; Zhao, D. Measuring the topological charge of optical vortices with a twisting phase. *Opt. Lett.* **2019**, *44*, 2334–2337. [CrossRef] [PubMed]
15. Ren, Y.; Wang, C.; Liu, T.; Wang, Z.; Yin, C.; Qiu, S.; Li, Z.; Wu, H. Polygonal shaping and multi-singularity manipulation of optical vortices via high-order cross-phase. *Opt. Express* **2020**, *28*, 26257–26266. [CrossRef] [PubMed]
16. Gu, B.; Wu, J.L.; Pan, Y.; Cui, Y. Achievement of needle-like focus by engineering radial-variant vector fields. *Opt. Express* **2013**, *21*, 30444–30452. [CrossRef]
17. Weng, X.; Gao, X.; Guo, H.; Zhuang, S. Creation of tunable multiple 3D dark spots with cylindrical vector beam. *Appl. Opt.* **2014**, *53*, 2470–2476. [CrossRef]

18. Man, Z.; Min, C.; Du, L.; Zhang, Y.; Zhu, S.; Yuan, X. Sub-wavelength sized transversely polarized optical needle with exceptionally suppressed side-lobes. *Opt. Express* **2016**, *24*, 874–882. [CrossRef]
19. Chen, Z.; Zhao, D. 4Pi focusing of spatially modulated radially polarized vortex beams. *Opt. Lett.* **2012**, *37*, 1286–1288. [CrossRef]
20. Wang, X.; Gong, L.; Zhu, Z.; Gu, B.; Zhan, Q. Creation of identical multiple focal spots with three-dimensional arbitrary shifting. *Opt. Express* **2017**, *25*, 17737–17745. [CrossRef]
21. Ouyang, X. Tight-focusing properties of the chirp modulation linearly polarized circular Airy Gaussian vortex beam. *Results Phys.* **2022**, *32*, 105119. [CrossRef]
22. Chen, Z.; Hua, L.; Pu, J. Tight focusing of light beams: Effect of polarization, phase, and coherence. *Prog. Optics. Elsevier* **2012**, *57*, 219–260.
23. Pu, J.; Zhang, Z. Tight focusing of spirally polarized vortex beams. *Opt. Laser Technol.* **2010**, *42*, 186–191. [CrossRef]
24. Lin, H.; Zhou, X.; Chen, Z.; Sasaki, O.; Li, Y.; Pu, J. Tight focusing properties of a circular partially coherent Gaussian beam. *JOSA A* **2018**, *35*, 1974–1980. [CrossRef] [PubMed]
25. Richards, B.; Wolf, E. Electromagnetic diffraction in optical systems. II. Structure of the image field in an aplanatic system. *Proc. R. Soc. Lond. A Math. Phys. Eng. Sciences. R. Soc.* **1959**, *253*, 358–379.
26. Kotlyar, V.V.; Nalimov, A.G. Analytical expression for radiation forces on a dielectric cylinder illuminated by a cylindrical Gaussian beam. *Opt. Express* **2006**, *14*, 6316–6321. [CrossRef]
27. Kotlyar, V.V.; Nalimov, A.G.; Stafeev, S.S. Focusing a vortex laser beam with polarization conversion. *Photonics* **2021**, *8*, 480. [CrossRef]
28. Lavanya, M.; Thiruarul, D.; Rajesh, K.B.; Mahadevan, G.; Velauthapillai, D.; Jaroszewicz, Z. Energy flux density for higher-order cylindrical vector vortex beam tightly focused through a dielectric interface. *J. Opt.* **2021**, *50*, 548–558. [CrossRef]
29. Kotlyar, V.V.; Stafeev, S.S.; Nalimov, A.G. Energy backflow in the focus of a light beam with phase or polarization singularity. *Phys. Rev. A* **2019**, *99*, 033840. [CrossRef]